

A TWO-STAGE INDUCTIVE VOLTAGE DIVIDER FOR COAXIAL BRIDGES

*G. A. Kyriazis*¹, *J. A. Moreno*², *J. Melcher*³

¹ Inmetro, Duque de Caxias, Brazil, gakyriazis@inmetro.gov.br

² CENAM, Querétaro, Mexico, jmoreno@cenam.mx

³ PTB, Braunschweig, Germany, juergen.melcher@ptb.de

Abstract: The traceability chain to derive the capacitance unit from the quantum Hall resistance comprises some coaxial bridges. These bridges employ a main two-stage inductive voltage divider to provide the voltage ratio needed. One such divider has recently been constructed and calibrated at Inmetro. The design techniques responsible for the small ratio errors of the device are detailed.

Keywords: inductive voltage dividers, coaxial bridges, traceability, guarding, two-stage techniques.

1. INTRODUCTION

The main inductive voltage divider (IVD) to be used in coaxial ratio bridges [1] should be constructed to provide an overall bridge uncertainty at 1:–1 and 10:–1 ratios of a few parts in 10⁸. This requires the use of special guarding and two-stage techniques typically adopted in the 10-100 kHz range [2].

A similar IVD had been constructed previously during the development of Inmetro's two terminal-pair coaxial capacitance bridge [3][4]. This bridge has been in operation since 2005. The IVD design details and calibration results had been reported in [5]. The new IVD discussed here was completely constructed at Inmetro and presents much smaller ratio errors than the previous one. We detail in section 2 the design changes that we believe were responsible for the results obtained. This work benefitted from the technical expertise of Centro Nacional de Metrología (CENAM) and Physikalisch-Technische Bundesanstalt (PTB). The IVD calibration is discussed in section 3. The old IVD was replaced by the new one in the coaxial capacitance bridge and the overall bridge uncertainty was reevaluated and reported in section 4. The conclusions are drawn in section 5.

2. DESIGN AND CONSTRUCTION

A schematic diagram showing the arrangement of cores, windings and guarding is shown in Fig. 1.

The IVD operates with up to 200 V (at 1 kHz) across the 0 and M10 taps. Therefore the first stage core comprises two plastic-encased supermalloy toroidal cores with 76.2 mm inner dia. x 101.6 mm outer dia. x 25.4 mm height and 0.0254 mm tape thickness (Magnetics 01500441F) placed one on top of the other. (Note: the previous design described in [5] used aluminum-encased cores).

A uniform one-layer 220-turn (with 0.57 mm dia. magnet wire) magnetizing winding covers the entire first stage core. This winding has three main taps for external connection whose leads are colored for easy identification, namely, 0 (red), M10 (blue) and M11 (black), which are equivalent to ratios 0, 1.0 and 1.1, respectively. The guard source for the divider winding is obtained by tapping the magnetizing winding at appropriate points (yellow). The guard source taps are equally spaced around the core (arranged in a star configuration – see Fig. 2). The guard voltages are 0.05 V, 0.15 V, 0.25 V ... 1.05 V (assuming 1 V input).

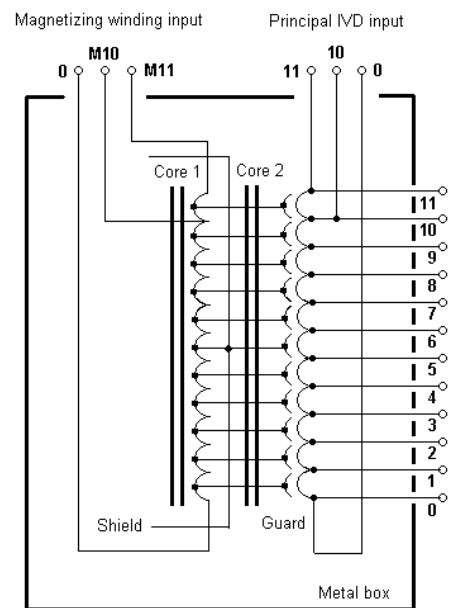


Fig. 1. Schematic diagram showing the arrangement of cores, windings, and guarding (the grounding conductors are not shown for clarity).

The magnetizing winding is covered with kapton tape (an insulating tape with good electrical, mechanical and thermal properties) and enclosed in a soldered toroidal shield made of 0.1 mm copper foil (Fig. 2). The shield is set at mid-tap potential, i.e. connected to the magnetizing winding tap corresponding to 0.55 ratio (see Fig. 1).

The cross-sectional area of the second stage core was chosen so that it has a magnetic permeance of about 1/3 that of the first stage core. Therefore two plastic-encased supermalloy toroidal cores with dimensions 76.2 mm inner dia. x 95.3 mm outer dia. x 9.5 mm height and 0.0254 mm

tape thickness (Magnetics 01500671F) were chosen. One core is placed on top of the shielded magnetizing winding and the other below it (Fig. 3). This symmetric arrangement was chosen to minimize leakage fields. (Note: both the first and the second stage cores had been enclosed together within the toroidal shield in the design described in [5]).

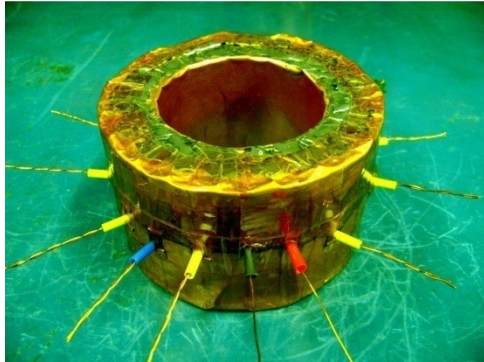


Fig. 2. Shielded magnetizing winding with guard source taps.

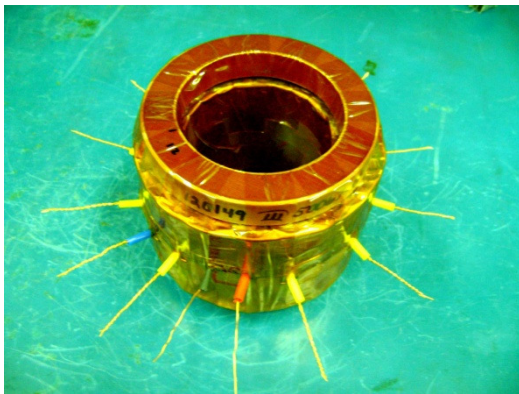


Fig. 3. Shielded magnetizing winding with second stage cores (a second stage core is located below the assembly and cannot be seen).

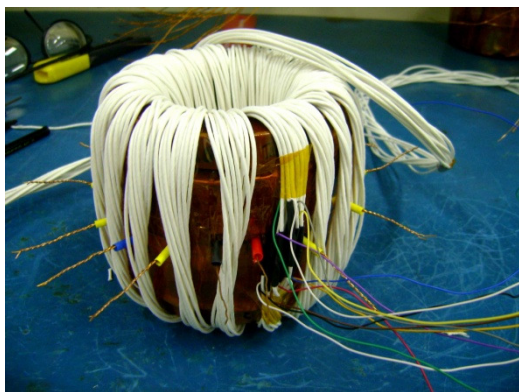


Fig. 4. Ratio winding (rope arrangement).

The IVD ratio winding consists of a 20-turn rope of 11 coaxial cables wound around the core assembly whose ends are connected in series to create a 220-turn winding (Fig. 4). (Note: here lies another difference from the previous design: a rope arrangement of the cables had not been employed in [5]). The tapped terminals 1 ... 10 are brought out from these interconnections (see Fig. 1). The centre conductor is tapped at ten points, which are equivalent to ratios 0.1, 0.2, 0.3 ... 1. The outer shield of the cable is cut (and insulated) at each

tap. In this type of construction each section has the same resistance and is equally well coupled to all other sections, thus balancing the mutual and leakage impedances.

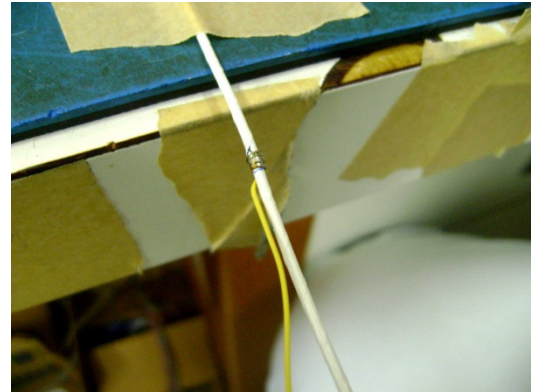


Fig. 5. A wire soldered to the middle of the outer conductor.

Before arranging the cables in a rope, a colored wire is soldered as accurately as possible to the middle of the outer conductor of each coaxial cable (Fig. 5). The whole assembly is then insulated with glass-fiber tape and the separate wires are connected to the corresponding magnetizing winding taps (Fig. 6). Colored wires are used to ensure that the wire is being connected to the correct guard tap. We confirmed that mistakes here are common and always result in large IVD ratio errors. This guarding method is an attempt to equalize the admittances between each half of each guard and nearby conductors.

The coaxial cable is GORE GSC 6591 (conductor size: 19 x 0.127 mm AWG 24 (19/36), 0.24 mm²; conductor material: CuAg, 78.5 mΩ/m; dielectric diameter: 0.84 mm; dielectric material: PTFE; screen details: braided screen from CuAg AWG 38 (1); jacket material: 0.15-mm PTFE; nominal diameter: 1.6 mm.).

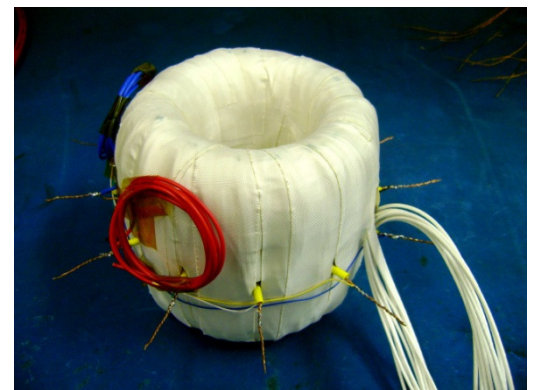


Fig. 6. Separate wires connected to the magnetizing winding taps.

The whole assembly is then insulated with kapton tape, isolated from mechanical vibrations (with 25 mm extruded polystyrene slabs fixed by two opposing insulating boards kept firm with four aluminum rods) and enclosed in a metal box with holes on its top panel for later penetration of the coaxial output sockets (Fig. 7).

The method of bringing out the taps to the coaxial connectors requires consideration if the highest possible accuracy is to be attained. The coaxial output sockets (BPO

connectors) are fixed to a rigid insulating board placed above the IVD assembly (Fig. 8). They are insulated from the metal box. Stout conductors (1.3 mm dia. magnet wire) are taken from the socket outers for the IVD ratio winding, routing them close to the short tap connections to a point well within the volume of the box where they are joined together (see Fig. 7). This point is grounded to the metal box through an output socket. The electrical resistance between each socket outer and the metal box was measured to be less than 0.015 Ω .

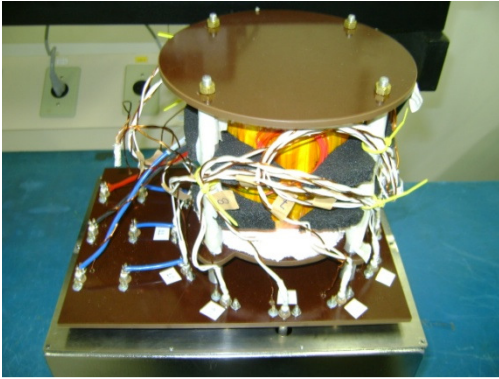


Fig. 7. The whole assembly is insulated from mechanical vibrations.

The same arrangement for bringing out the taps to the coaxial connectors is adopted for the IVD magnetizing winding leads. The joint point of the stout conductors is also grounded to the metal box through another output socket. The resistance between each socket outer and the metal box was measured to be less than 0.009 Ω . The BPO connectors for the magnetizing winding are the three ones located in the right side of Fig. 8. See [1] for more details on this grounding arrangement.

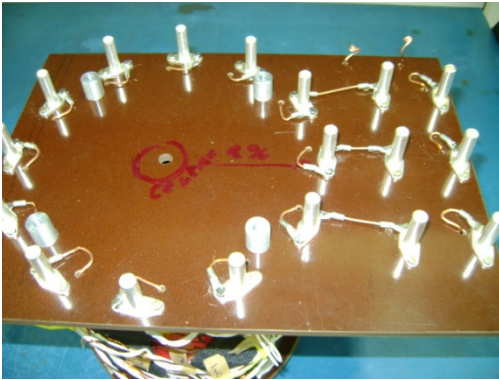


Fig. 8. Coaxial output sockets (BPO connectors).

The metal box is made of 1.5 mm chromium-coated carbon steel and the box inner surface is covered with 0.79 mm mumetal sheets. The box panel has the following outputs: (a) divider taps: 0 (twofold), 1, 2, 3, 4, 5, 6, 7, 8, 9, 10 (twofold), and 11 (twofold), (b) magnetizing winding taps: 0, M10 and M11, and (c) two independent ground connections (both the magnetizing winding and the ratio winding stout conductor joint points were always grounded to the metal box in the IVD calibration and capacitance bridge measurements – see ref. [3]). The final assembly of the main IVD is shown in figure 9. The short-circuiting

plugs of the two independent ground connections are not shown in the figure.



Fig. 9. Main IVD final assembly.

3. CALIBRATION

The IVD 10:–1 ratio error was calibrated at Inmetro. The old IVD was replaced by the new one in the coaxial capacitance bridge (see [3][4] for constructional details of this bridge) and the bridge was used to compare 10 pF and 100 pF fused-silica standard capacitors which had been previously calibrated by BIPM with a relative uncertainty of 4 parts in 10^8 . With this method one can only measure the in-phase component of the complex ratio error. The calibration was performed at 110 V (across the 0 and M11 taps) and at both 1 kHz and 1.592 kHz.

3.1. Measurement model

The simplified scheme of the capacitance bridge is shown in Fig. 10. The main IVD operates with a voltage U across the 0 and 1 taps for the 1:–1 ratio or across the 0 and 1.1 taps for the 10:–1 ratio. The voltage value depends on the bridge ratio and the standard capacitor value (Table I). The value of ratio $1/v$ depends on the bridge ratio and the voltage predivider ratios (Table II). The resulting dividing factors of the bridge main balance are $\alpha = (a - 0.5)/0.5$ and $\beta = (b - 0.5)/0.5$, where a and b are the settings of each six-decade main balance IVD. See [3] for predivider and balance IVD details. The nominal ratio of the main IVD is $D = 1/2$ for the 1:–1 ratio and $D = 1/11$ for the 10:–1 ratio. Here we want to determine the in-phase component of the complex ratio error ε from the known values of capacitors C_N (with unknown conductance G_N) and C_X (with unknown conductance G_X). C is a 1 pF fused-silica standard capacitor. G and C' are the conductance and parasitic capacitance, respectively, of a T-network box (with connecting cables), measured with a commercial capacitance bridge.

The ratio error is here expressed as a fraction of unit. In this case, the IVD ratio is expressed as a sum of the nominal ratio D and of the complex ratio error $k' + jk''$ (k' and k'' are respectively the in-phase and quadrature components),

$$U_{0,1-0} / U_{1,1-0} = D + \varepsilon = D + k' + jk'' \quad (1)$$

The main balance is obtained when

$$\mathbf{I}_N + \mathbf{I}_X + \mathbf{I}_B = \mathbf{I}_M = 0 \quad (2)$$

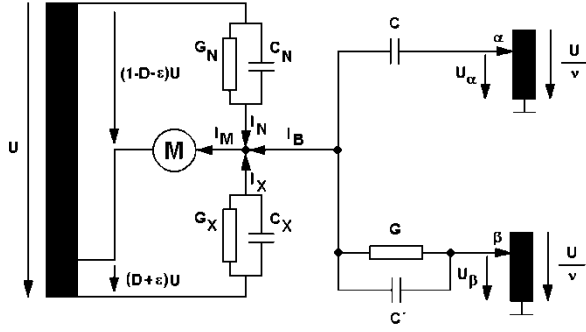


Fig. 10. Simplified scheme of the capacitance bridge.

The balance equation for the 1:-1 ratio is

$$C_X = C_N + (\alpha_1 - \alpha_2) \frac{C}{v} + (\beta_1 - \beta_2) \frac{C'}{v} \quad (3)$$

The dividing factors α_1 and β_1 are obtained by balancing the bridge with the capacitors positioned as shown in Fig. 10, and α_2 and β_2 are obtained by rearranging the cables so that the capacitors are in the reversed position. The complex ratio error of the main IVD is cancelled out by this technique. It is interesting however to compute the complex ratio error of the main IVD for the 1:-1 ratio, that is

$$k' = \frac{1}{4v} \left[\frac{C}{C_N} (\alpha_1 + \alpha_2) + \frac{C'}{C_X} (\beta_1 + \beta_2) \right] \quad (4)$$

$$k'' = -\frac{G}{4\omega v C_N} (\beta_1 + \beta_2)$$

This is typically done for quality control purposes.

Table I. Total applied voltage U .

C_N (pF)	Bridge ratio	U (V)
10	1:-1	200
10	10:-1	110
100	1:-1	20
100	10:-1	11
1000	1:-1	2

Table II. Value of v .

Predivider ratio	Bridge ratio	v
10:-1	1:-1	100
10:-1	10:-1	110
1:-1	1:-1	10
1:-1	10:-1	11

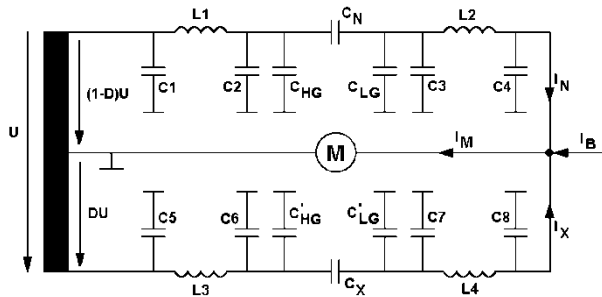


Fig. 11. Bridge simplified scheme with cable modeling.

The balance equation for the 10:-1 ratio is

$$C_X = C_N \left(\frac{1-t}{t} \right) (1 + \Delta_g) \quad (5a)$$

where

$$t = D + k'$$

$$\Delta_g = \Delta_c + \Delta_{c'} + \Delta_{k'}$$

$$\Delta_c = \frac{C}{C_N} \left(\frac{\alpha}{v(1-t)} \right) \quad (5b)$$

$$\Delta_{c'} = \frac{C'}{C_N} \left(\frac{\beta}{v(1-t)} \right)$$

$$\Delta_{k'} = -\frac{k''}{t(1-t)} \left(\tan \delta_N + \frac{\beta G}{\omega v C_N} \right)$$

where ω is the angular frequency and $\tan \delta_N$ is the loss tangent of C_N . Here it is neither possible nor necessary to use the aforementioned cabling reversal technique.

The dividing factors α and β can be expressed as

$$\alpha = \bar{\alpha} + R_\alpha + \sigma_\alpha \quad (6)$$

$$\beta = \bar{\beta} + R_\beta + \sigma_\beta$$

where $\bar{\alpha}$ and $\bar{\beta}$ are the values, R_α and R_β are the resolutions and σ_α and σ_β are the random deviations of the α and β readings, respectively.

Neglecting the contribution from $\Delta_{k''}$, and rearranging terms, the IVD ratio can be expressed as

$$t = \frac{C_N + A}{C_N + C_X} \quad (7)$$

where

$$A = \frac{1}{v} (C\alpha + C'\beta) \quad (8)$$

The values of C_N and C_X in (5) include their drifts with time and the cable parasitic contributions. We must first correct the capacitance values for the cable errors. A simplified scheme of the capacitance bridge with the connecting cables modeled as delta networks is shown in Fig. 11. As high quality cables are used cable losses can be neglected here.

L_1 and C_2 are, respectively, the inductance and half the capacitance of the cable that connects C_N to the main IVD (see Fig. 10). L_3 and C_6 are, respectively, the inductance and half the capacitance of the cable that connects C_X to the main IVD. The contribution of C_1 (and C_5) is not taken into account since these capacitances are in parallel with the source. The contribution of C_4 (and C_8) is negligible when the bridge is balanced. L_2 and C_3 are, respectively, the inductance and one-fourth the capacitance of the cable that connects C_N to the bridge null. L_4 and C_7 are, respectively, the inductance and one-fourth the capacitance of the cable that connects C_X to the bridge null. C_{HG} and C_{LG} are the parasitic capacitances to ground of the high and low inputs

of C_N , respectively. C'_{HG} and C'_{LG} are the capacitances to ground of the high and low inputs of C_X , respectively.

The cable relative error for C_N is approximately

$$\varepsilon_{RN} = \frac{C_{TN} - C_N}{C_N} \approx \omega^2 [L_1(C_N + C_{2HG}) + L_2(C_N + C_{3LG})] \quad (9)$$

where C_{TN} is the total capacitance of C_N (capacitor plus cables), $C_{2HG} = C_2 + C_{HG}$ and $C_{3LG} = C_3 + C_{LG}$.

The cable relative error for C_X is approximately

$$\varepsilon_{RX} = \frac{C_{TX} - C_X}{C_X} \approx \omega^2 [L_3(C_X + C'_{6HG}) + L_4(C_X + C'_{7LG})] \quad (10)$$

where C_{TX} is the total capacitance of C_X (capacitor plus cables), $C'_{6HG} = C_6 + C'_{HG}$ and $C'_{7LG} = C_7 + C'_{LG}$.

Hence,

$$\begin{aligned} C_N &= \bar{C}_N (1 + \varepsilon_{RN}) + d_N \\ C_X &= \bar{C}_X (1 + \varepsilon_{RX}) + d_X \end{aligned} \quad (11)$$

where \bar{C}_N and \bar{C}_X are the capacitance values reported in the calibration certificate, ε_{RN} and ε_{RX} are the relative corrections of the cables connected to each capacitor, and d_N and d_X are the capacitor drifts in the period between the date the capacitor calibration certificates were issued by BIPM and the date of the IVD calibration. We regard both the standard capacitor and its associated cable as a whole standard. The value of C_N is therefore inserted in the spreadsheet as $C_N(1 + \varepsilon_{RN})$ and the value of C_X is inserted in the spreadsheet as $C_X(1 - \varepsilon_{RX})$.

Since the main uncertainty contributions to the cable error are associated with the parasitic inductances and capacitances of the capacitor and cable, we may neglect the uncertainty contribution associated with the capacitor values and write

$$\begin{aligned} C_N &= \bar{C}_N + \delta C_N + d_N \\ C_X &= \bar{C}_X + \delta C_X + d_X \end{aligned} \quad (12)$$

where δC_N and δC_X are the absolute corrections of the cable errors (in F), that is

$$\delta C_N \approx \omega^2 C_N [L_1(C_N + C_{2HG}) + L_2(C_N + C_{3LG})] \quad (13a)$$

$$\delta C_X \approx \omega^2 C_X [L_3(C_X + C'_{6HG}) + L_4(C_X + C'_{7LG})] \quad (13b)$$

Here $C_N = 10$ pF and $C_X = 100$ pF, and it is assumed that their contributions to the uncertainty associated with δC_N and δC_X are negligible.

3.2. Measurement uncertainty

It is important to observe that the variables \bar{C}_N and \bar{C}_X are strongly correlated as the capacitors were calibrated at BIPM with the same system. Therefore,

$$u(\bar{C}_N, \bar{C}_X) \neq 0 \quad \Rightarrow \quad u(C_N, C_X) \neq 0 \quad (14)$$

The squared standard uncertainty associated with the IVD ratio is then [6]

$$\begin{aligned} u^2(t) &= \frac{(C_X - A)^2}{(C_N + C_X)^4} \cdot u^2(C_N) + \frac{(C_N + A)^2}{(C_N + C_X)^4} \cdot u^2(C_X) \\ &\quad + \frac{1}{(C_N + C_X)^2} \cdot u^2(A) - 2 \cdot \frac{(C_X - A)(C_N + A)}{(C_N + C_X)^4} \cdot u(C_N, C_X) \end{aligned} \quad (15)$$

where,

$$u^2(C_N) = u^2(\bar{C}_N) + u^2(\delta C_N) + u^2(d_N)$$

$$u^2(C_X) = u^2(\bar{C}_X) + u^2(\delta C_X) + u^2(d_X)$$

$$\begin{aligned} u^2(\delta C_N) &= \omega^2 C_N^2 u^2(L_1) + \omega^2 C_N u^2(C_{2HG}) + \omega^2 C_N^2 u^2(L_2) \\ &\quad + \omega^2 C_N u^2(C_{3LG}) \end{aligned}$$

$$\begin{aligned} u^2(\delta C_X) &= \omega^2 C_X^2 u^2(L_3) + \omega^2 C_X u^2(C'_{6HG}) + \omega^2 C_X^2 u^2(L_4) \\ &\quad + \omega^2 C_X u^2(C'_{7LG}) \end{aligned}$$

$$\begin{aligned} u^2(A) &= \frac{1}{v^2} [C^2 u^2(\alpha) + \alpha^2 \cdot u^2(C) + C'^2 u^2(\beta) + \beta^2 u^2(C')] \\ &\quad + \frac{1}{v^4} \cdot (C\alpha + C'\beta)^2 u^2(v) \end{aligned}$$

$$u^2(\alpha) = u^2(\bar{\alpha}) + u^2(R_\alpha) + u^2(\sigma_\alpha)$$

$$u^2(\beta) = u^2(\bar{\beta}) + u^2(R_\beta) + u^2(\sigma_\beta)$$

$$u(C_N, C_X) = u(\bar{C}_N, \bar{C}_X) = u(\bar{C}_N) \cdot u(\bar{C}_X)$$

since a correlation $\rho(\bar{C}_N, \bar{C}_X) = 1$ is assumed here.

3.3. IVD calibration results

The in-phase 10:–1 ratio errors k' and their expanded uncertainties $U(k')$ evaluated respectively from (7) and (15) are listed in Table III. Table IV lists the in-phase and quadrature 1:–1 ratio errors evaluated from (4).

Table III. In-phase 10:–1 ratio errors (new IVD).

Frequency (Hz)	k'	$U(k')$
1000	3×10^{-9}	23×10^{-9}
1592	12×10^{-9}	23×10^{-9}

Table IV. In-phase and quad 1:–1 ratio errors (new IVD).

Frequency (Hz)	k'	k''
1592	23×10^{-9}	9×10^{-9}

The old IVD whose construction was reported in [5] was calibrated again using the same method described here. The reader should compare the results listed in Table V and VI with those for the new IVD.

Table V. In-phase 10:–1 ratio errors (old IVD).

Frequency (Hz)	k'	$U(k')$
1000	-124×10^{-9}	23×10^{-9}
1592	-164×10^{-9}	23×10^{-9}

Table VI. In-phase and quad 1:–1 ratio errors (old IVD).

Frequency (Hz)	k'	k''
1592	-280×10^{-9}	23×10^{-9}

The ratio errors of the new IVD are indeed much smaller.

4. COAXIAL CAPACITANCE BRIDGE

The new IVD was installed in the two terminal-pair coaxial capacitance bridge and the uncertainty obtained in capacitance calibration was assessed again here. This bridge has been used at Inmetro for calibrating stable standard capacitors since its construction in 2005.

An experiment was made recently to evaluate the consistency of the measurement results obtained with this bridge. Consider three 10 pF fused-silica standard capacitors labeled here for convenience as A, B, and C. Capacitor A is traceable to BIPM. Firstly, capacitor B was calibrated by comparing it with known capacitor A. Secondly, capacitor C was similarly calibrated and the (computed) difference between B and C values was recorded. Capacitor B (assuming it to be unknown) was then calibrated by comparing it with the (now) known capacitor C and the (measured) difference between B and C values was also recorded. All measurement results were corrected for cable errors. The computed and measured differences between B and C values differed by 7×10^{-10} at 1.592 kHz when the new IVD was installed in the bridge. Contrast this with the 6.7×10^{-9} figure obtained when the old IVD was installed in the bridge (or even with the 1.5×10^{-8} figure reported earlier in [3]). This is a bridge systematic error which is detected when comparing several standards of same nominal value for consistency in the results. This error contributes to the overall uncertainty of the bridge at 1:–1 ratio. So, this uncertainty contribution was reduced by one order of magnitude as a result of the reduced ratio errors presented by the new IVD.

Table VII. Uncertainty budget (10 pF – 1.592 kHz).

Quantity	Standard uncertainty	Sensitivity coefficient	Eval. Type
$C_N^{(1)}$	4.0×10^{-7} pF	1	B
$\Delta\alpha$	3.16×10^{-6}	1.00×10^{-2} pF	A
$\Delta\beta$	7.48×10^{-7}	8.00×10^{-6} pF	A
C	4×10^{-8} pF	6.56×10^{-5}	B
C'	0.0008 pF	8.00×10^{-7}	B
v	0.1	6.63×10^{-7} pF	B
$\epsilon_R^{(2)}$	1×10^{-8} pF	1	B
$C_X - C_N^{(3)}$	7×10^{-8} pF	1	Comb.
Error ⁽⁴⁾	7×10^{-9} pF	1	B
$C_X^{(5)}$	7×10^{-8} pF	1	Comb.
$R_{K-90}^{(6)}$	1.00×10^{-6} pF	1	B
Biannual Drift ⁽⁷⁾	1.00×10^{-6} pF	1	A
$C_X^{(8)}$	1.5×10^{-6} pF		Comb.

⁽¹⁾ Relative combined standard uncertainty reported in the BIPM calibration certificate for C_N (a 10 pF capacitor).

⁽²⁾ Uncertainty contribution associated with the correction for the cable errors.

⁽³⁾ Combined standard uncertainty associated with the difference between the capacitances of the standards being compared (see text).

⁽⁴⁾ Systematic error that is detected when comparing several standards for consistency in the results.

⁽⁵⁾ Combined standard uncertainty associated with C_X without taking into account the uncertainty contributions associated with R_{K-90} and the reference standard biannual drift. C_X is a 10 pF capacitor.

⁽⁶⁾ Standard uncertainty associated with the recommended value of R_{K-90} .

⁽⁷⁾ Drift evaluated by fitting a straight line to data reported in BIPM calibration certificates in the last six years.

⁽⁸⁾ Combined standard uncertainty associated with C_X by taking into account all known uncertainty contributions.

Table VII shows the uncertainty budget for the calibration at 1:–1 ratio and at 1.592 kHz of a stable 10 pF fused-silica standard capacitor (C_X) from a similar capacitor (C_N) traceable to BIPM. The combined relative standard uncertainty associated with the difference between the capacitance values of the standards being compared ($C_X - C_N$) is less than one part in 10^8 . The uncertainty contribution due to the capacitance bridge is therefore negligible compared to other contributions such as the relative uncertainty reported in the BIPM certificate, the reference standard drift, and the uncertainty associated with the recommended value of R_{K-90} (von Klitzing constant). The major uncertainty contributions are now the 1/v ratio and the stability of the $\Delta\alpha$ ($= \alpha_1 - \alpha_2$) readings.

Table VIII. Uncertainty budget (100 pF – 1.592 kHz).

Quantity	Standard uncertainty	Sensitivity coefficient	Eval. Type
$C_N^{(1)}$	4.0×10^{-7} pF	10	B
α	1.5×10^{-6}	1.00×10^{-1} pF	A
k'	1.2×10^{-8}	-1.21×10^5	B
$\epsilon_R^{(2)}$	1×10^{-8} pF	1	B
$C_X^{(3)}$	1.51×10^{-5} pF	1	Comb.
$R_{K-90}^{(4)}$	1.00×10^{-5} pF	1	B
Biannual Drift ⁽⁵⁾	1.00×10^{-5} pF	1	A
$C_X^{(6)}$	2.1×10^{-5} pF		Comb.

⁽¹⁾ Relative combined standard uncertainty reported in the BIPM calibration certificate for C_N (a 10 pF capacitor).

⁽²⁾ Uncertainty contribution associated with the correction for the cable errors.

⁽³⁾ Combined standard uncertainty associated with C_X without taking into account the uncertainty contributions associated with R_{K-90} and the reference standard biannual drift. C_X is a 100 pF capacitor.

⁽⁴⁾ Standard uncertainty associated with the recommended value of R_{K-90} .

⁽⁵⁾ Drift evaluated by fitting a straight line to data reported in BIPM calibration certificates in the last six years.

⁽⁶⁾ Combined standard uncertainty associated with C_X by taking into account all known uncertainty contributions.

Table VIII shows the uncertainty budget for the calibration at 10:–1 ratio and at 1.592 kHz of a stable 100 pF fused-silica standard capacitor (C_X) from a similar 10 pF capacitor (C_N) traceable to BIPM. The combined relative standard uncertainty associated with the calibration result (without the uncertainty contributions associated with R_{K-90} and with the reference standard drift) is 1.5×10^{-7} . The major contribution to the overall bridge uncertainty at the 10:–1 ratio is that associated with the in-phase component of the IVD ratio error.

As mentioned in the introduction, the main IVD to be used in coaxial ratio bridges should be constructed to provide an overall bridge uncertainty at 1:–1 and 10:–1 ratios of a few parts in 10^8 . In order to achieve this for the 10:–1 ratio it is necessary to reduce the uncertainty associated with the IVD in-phase ratio error by one order of magnitude. This demands the construction of a special system for calibrating the IVD 10:–1 ratio with an uncertainty of a few parts in 10^9 .

Note: Quantities not listed in Tables VII and VIII were found to have negligible uncertainty contributions.

5. CONCLUSION

The constructional details of the new IVD recently built at Inmetro were presented along with the design changes implemented. The design changes are: (a) plastic-encased cores are used as first stage cores, (b) only the magnetizing winding and the first stage cores are copper shielded and (c) a rope arrangement is employed for the coaxial cables in the ratio winding. The method used to calibrate the IVD ratio error was also described in detail. The in-phase 10:–1 ratio error was determined from known values of two stable decadic standard capacitors.

It was confirmed that the ratio errors of the new IVD are much smaller than those reported previously for another IVD. Upon installing the new IVD in the coaxial capacitance bridge, the major contributions to the overall uncertainty of the 1:–1 ratio bridge are those associated with the predivider ratio and with the stability of the readings. The major contribution at 10:–1 ratio is that associated with the in-phase component of the IVD ratio error. A special system for calibrating the IVD 10:–1 ratio with an uncertainty of a few parts in 10^9 is required if one needs to achieve an overall uncertainty of parts in 10^8 with the 10:–1 ratio bridge.

REFERENCES

- [1] B. P. Kibble and G. H. Rayner, *Coaxial AC Bridges*, Adam Hilger Ltd., 1984.
- [2] D. Homan and T. Zapf, "Two stage, guarded inductive voltage divider for use at 100 kHz", *ISA Trans.*, Vol. 9, no. 3, pp. 201-209, 1970.
- [3] G.A. Kyriazis, R.T.B. Vasconcellos, L.M. Ogino, J. Melcher and J. A. Moreno, "Design and construction of a two terminal-pair coaxial capacitance bridge", in *Proc. of the VI SEMETRO*, pp. 57-62, Rio de Janeiro, 2005.
- [4] G. A. Kyriazis, R. T. B. Vasconcellos, L. M. Ogino, J. Melcher and J. A. Moreno, "A two terminal-pair coaxial capacitance bridge constructed at Inmetro", in *CPEM Digest*, pp. 522-523, Turin, 2006.
- [5] G.A. Kyriazis, J. Melcher and J.A. Moreno, "A two-stage, guarded inductive voltage divider for use in coaxial bridges employed in the derivation of the capacitance unit from quantized Hall resistance", in *CPEM Digest*, pp. 131-132, London, 2004.
- [6] BIPM, IEC, IFCC, ISO, IUPAC, IUPAP and OIML, *Guide to the Expression of Uncertainty in Measurement*, Geneva, Switzerland: Int. Org. Standardization, 1995.